International Journal of Automotive Technology, Vol. 20, No. 2, pp. 365−377 (2019)
DOI 10.1007/s12239−019−0036−5
Copyright © 2019 KSAE/ 107−16
pISSN 1229−9138/ eISSN 1976−3832

ONLINE MEASURING METHOD FOR THE ENGINES' IVC TIMING BASED ON THE IN-CYLINDER PRESSURE FLUCTUATION

Fushui Liu[1, 2], Zhongjie Shi[1], Yikai Li[1)*], Yang Hua[1], Yanlin Chen[1] and Yongli Gao[1]

[1]School of Mechanical Engineering, Beijing Institute of Technology, Beijing 100081, China
[2]Beijing Electric Vehicle Collaborative Innovation Center, Beijing 100081, China

(Received 28 May 2018; Revised 6 August 2018; Accepted 11 October 2018)

ABSTRACT−The in-cylinder pressure fluctuations caused by intake valve closure (IVC) event were first investigated experimentally based on a single cylinder diesel engine with different cams. The experimental results show that the occurrence of the in-cylinder pressure fluctuation during the compression stroke has a close correlation with the IVC event. The start time of the pressure oscillation advances as the IVC timing advances. With a fixed IVC timing, higher engine speed results in a larger fluctuation amplitude and a longer fluctuation duration. To explain these phenomena, a numerical simulation model has been adopted. Results show that the IVC event causes pressure oscillations in both the cylinder and intake runner. At the same engine speed, the amplitude of the pressure oscillation decreases first and then increases as the IVC retards due to the change of gas flow direction. With the same intake temperature, the absolute time delay keeps constant at different engine speeds and IVC timings. The absolute time delay decreases as the intake temperature decreases. Based on the conclusions above, the potential methods to use the pressure oscillation are also discussed. An innovative engine valve timing detection method on the basis of in-cylinder pressure oscillation is presented.

KEY WORDS : Internal combustion engines, Online measuring, Valve events timing, Pressure fluctuation, CFD analysis

NOMENCLATURE

3D	: three dimentional
c	: speed of sound, m/s
CAD	: crank angle degree
CAI	: controlled auto-ignition
CFD	: computational fluid dynamics
CFLmach	: maximum Mach Courant Friedrichs-Lewy
CRe	: effective compression ratio
Δx	: grid length, m
Δt	: time step, s
ΔT	: time delay, s
FDD	: fault detection and diagnosis
FFT	: fast Fourier transformation
FNN	: probabilistic neural networks
γ	: adiabatic coefficient
HCCI	: homogeneous compression charge ignition
IC	: internal combustion
IVC	: intake valve closure
PCCI	: premixed compression charge ignition
R	: the gas constant, 287 J/(kg·K)
SOC	: start of combustion
VVA	: variable valve actuation
WVD	: Wigner–Ville distributions

**Corresponding author.* e-mail: liyikai@bit.edu.cn

1. INTRODUCTION

Increasingly stringent vehicle emission and fuel economy regulations worldwide have led to the applications of several innovative technologies, such as the variable valve actuation (VVA), high pressure injection, after treatment, Atkinson cycle, controlled auto-ignition (CAI), premixed compression charge ignition (PCCI) and homogeneous compression charge ignition (HCCI) (Brijesh and Sreedhara, 2013; Li *et al*., 2013; Liu *et al*., 2014; Lu *et al*., 2011; Peng and Jia, 2009; Yao *et al*., 2009). Among these new technologies, the Atkinson cycle and the new combustion strategies (PCCI/HCCI) were demonstrated to be capable of simultaneously reducing fuel consumption and emissions (Xu *et al*., 2017; Yao *et al*., 2009). As to the Atkinson cycle, the IVC timing adjusting is considered as a practical way to control the engine's effective compression ratio (CRe), and hence the engine thermal performance (Liu *et al*., 2014). As to the PCCI, and HCCI engines, which are featured with early in-cylinder fuel injection, it is difficult to control the auto-ignition timing owing to the high reactivity of the diesel fuel and the spontaneous combustion of the premixed fuel/air mixture (Li *et al*., 2013; Lu *et al*., 2011; Peng and Jia, 2009; Yao *et al*., 2009). Due to its fast-response characteristics and great influence on the CRe, the IVC adjusting strategy is considered as one of the most promising techniques to control the start of

combustion (SOC) of these engines (Jia *et al*., 2011, 2013; Liu *et al*., 2018; Mahrous *et al*., 2009; Milovanovic *et al*., 2004; Walter *et al*., 2008). Because CRe can vary during transient conditions due to the high range of the engine speed, online detection of the IVC is required in these engines to control the SOC predictively and precisely.

Furthermore, even for the produced engines featuring with VVA technology, due to the metal heat bilges, the reserved valve clearance, and the gradual deterioration of the engine and the valve train system, there exists a discrepancy between the engine's real valve timing (the valve events when the engine is running) and the designed one. Hence, online detecting of the IVC is required to maintain the engine's performance well during engine's life time.

Up to now, as the measure of vibration signals is comparatively simple and convenient, several previous studies have been performed concentrating on the detecting of the internal combustion (IC) engine valve train fault by analyzing the vibration signals measured at engine block or engine head. Ftoutou *et al*. (2011) used the time domain features extracted from vibration signals measured at several points on the engine block to classify the valve clearance fault in an IC engine. Justin Flett (Flett and Bone, 2016) compared five classification methods experimentally with a diesel IC engine and found that the FDD (fault detection and diagnosis) system using the Naïve-Bayes classification method produced the best overall performance with a lower detection accuracy of 99.95 %. To sort the vibration signals, the method proposed by these papers share a common characteristic: they all need extract feature parameters from the highly transient and non-stationary vibration signals. As this process may be a big load for the electric control unit, detecting the valve fault by extracting feature parameters is not realistic in the real engine. Wang *et al*. (2008) applied WVD (Wigner–Ville distributions) time frequency method to analyze the cylinder head vibration signals and performed FNN (probabilistic neural networks) classification method to diagnose the valve train fault. It has been found that, with no need to extract further fault features, this method is a more convenient and effective way to detect the engine's abnormal valve clearance. These studies as shown above compared the abnormal vibration signals with the normal ones, and then diagnosed the fault of the engine.

Another way to identify the mechanical valve movements in a running multi-cylinder diesel engine is the acoustic emission (AE) signals, which have an excellent signal-to-noise ratio in its frequency range (0.1 ~ 1 MHz), and allow discrimination of the fine detail of the fluid-mechanical events during each cycle (Reuben, 1998). Fog *et al*. (1999) carried out experimental AE investigations of exhaust valve leakage on a two-stroke marine diesel engine. Results from his measurements show that AE signals have a major advantage for monitoring reciprocating machinery.

Nevertheless, the application of vibration-based or AE-based IVC detecting to IC engines is rare. For vibration-based IVC detecting method, this is essentially because the vibration signals are susceptible to other vibration signals, such as combustion noise, transmission shift noise, and injector seating noise. This situation is deteriorated in the diesel engine whose noise is notorious before. In other words, the vibration signals are easily overwhelmed by other unrelated ones (Li *et al*., 2010). For AE-based IVC detecting method, this is because the AE signals the sensors acquired are highly dependent on the geometry of the engine block or the engine head. And it remains a big challenge in sensor calibration to provide a meaningful measurement due to the very complicated shape of the engine (Nivesrangsan *et al*., 2005, 2007a, 2007b; Wu *et al*., 2015).

The engine in-cylinder pressure fluctuations are also commonly used to monitor the engine conditions (Hickling *et al*., 1979). In gasoline engines, especially those with high compression ratio, the pressure fluctuation is easily occurred, known as "knock". When the end mixture in the chamber self-ignites due to the compression of the burned gas or the "hotspots" at the chamber wall, there exists a sharp pressure rise in the self-igniting region. Then the pressure waves propagate and reflect back and forth, and the knock happens. As the knock is harmful to the engine performance, especially to the reliability, it has attracted a lot of researchers (Beccari *et al*., 2016; Bozza *et al*., 2016; Tougri *et al*., 2017; Vafamehr *et al*., 2016) to study its mechanics. As for the diffusion combustion diesel engine, at the early stage of the combustion, several regions of premixed mixture react simultaneously and fast, and cause a quick rise of the local pressure. Then, the high frequency pressure oscillation happens (Kyrtatos *et al*., 2016; Zhang *et al*., 2017). Zhang *et al*. (2017) analyzed the energy and time-frequency distribution of the tested in-cylinder pressure oscillation in a muti-injection diesel engine, concluded that the pilot injection is more important for pressure oscillation in each combustion stage than the main injection.

Several previous studies have been performed concentrating on the estimation of the engine parameters by using the in-cylinder pressure fluctuations. The first attempt was done by Hickling *et al*. (1983) who used the resonant frequency for estimating the bulk temperature in a heavy-duty Diesel engine. In 2012, Bodisco *et al*. (2012) employed a Bayesian characterization of the HCCI pressure fluctuations in order to simulate the resonant frequency evolution during a cycle, which is later used for inferring bulk temperature of the gas and the trapped mass. More recently, José Manuel (Luján *et al*., 2016) proposed a convenient method to estimate the trapped mass by identifying the resonant frequency of the in-cylinder pressure waves on a HCCI engine. However, previous papers dealing with the in-cylinder pressure fluctuations are focused on the combustion noise.

Throughout all of the literatures above, the studies on the valve monitoring focuses on the vibration signals or AE signals, both are originated from the impacts between the valves and the engine body. While, the studies on the in-cylinder pressure fluctuations focuses on fluctuations caused by the combustion, ignoring the pressure fluctuations caused by intake events during engine ventilation process. In IC engines, the IVC event stops the high-speed air that is entering or leaving the cylinder suddenly, and this may cause the pressure oscillations in the cylinder. Detecting the IVC timing based on the in-cylinder pressure oscillation can avoid the other unrelated vibration signals and has no relation to the complicated shape of the engine. However, to the best of our knowledge, there were no detailed characteristics of in cylinder pressure oscillation which is excited by IVC event being revealed in previous works. For this reason, this paper investigates the effects of IVC on the in-cylinder pressure oscillation and presents a new method to determine the IVC event of the diesel engine based on the in-cylinder pressure fluctuations.

The purpose of this paper is to study the detailed characteristics of the in-cylinder pressure fluctuations that caused by the valve event and the effects of the engine operating conditions on them. The main objective is to establish the hysteresis relationship between the engine valve event and the pressure fluctuations in the cylinder under different operating conditions and to measure the IVC timing during the working condition of the engine.

For this purpose, a single-cylinder diesel engine equipped with different cams was used to study the pressure fluctuation characteristics in the cylinder during the ventilation process and the effect of the engine speed and the IVC on the pressure oscillations. In order to further explore the detailed information of the pressure wave, the three dimentional (3D) computational fluid dynamics (CFD) model was used to reproduce the pressure oscillations in the cylinder. The effects of intake air temperature and IVC on the pressure oscillation characteristics were also studied. The relationship between the IVC and the pressure oscillations was established.

2. METHODOLOGY AND PROCESS

2.1. Experimental Apparatus

The experiments were performed on a four-valve single-cylinder diesel research engine, with a cylinder bore of 132 mm, stroke length of 145 mm and connecting rod length of 262 mm. The compression ratio is 13.5. The specifications of the engine are detailed in Table 1.

The schematic diagram of experimental setup is shown in Figure 1. The dynamometer system mainly consists of an eddy current dynamometer (provided by Maikai) and a Siemens frequency converter. The pressure charging system included a VHN-16/8 piston compressor, a buffer tank, a heat exchanger and several pipes. The Kistler 4007B sensor was used to obtain the instantaneous absolute pressure of intake and exhaust manifold. The in-cylinder pressure was measured by Kistler 6025B piezoelectric sensor which was installed on the engine head with a precision of ± 0.1 bar. The piezoelectric sensor was mounted directly exposed to the chamber so that the cavity effects could be minimized. Intake air flow rate was measured by an Air Flow Meter with a precision of 1 %. A CMFD010 Fuel Consumption Meter was used to measure the fuel consumption of the engine. Details about the experiment system can be found in the reference (Li *et al.*, 2016).

Table 1. Engine specifications.

Engine	Four-stroke
Displaced volume	1984 cc
Stroke	145 mm
Bore	132 mm
Connecting rod	262 mm
Compression ratio	13.5 : 1
Number of valves	4
Exhaust valve open	34 BBDC @ 0.3 mm lift
Exhaust valve close	6 ATDC @ 0.3 mm lift
Intake valve open	2 BTDC @ 0.25 mm lift
Intake valve close	34 ABDC @ 0.25 mm lift

In the single cylinder diesel engine experiment, the intake valve opening, and exhaust valve closure and opening points were kept fixed during all tests. The intake air temperature was controlled at 333 K. Initially, tests were carried at full load with different speeds of 1600 r/min. 1900 r/min, 2100 r/min, and 2500 r/min. Then, the IVC timing was changed by switching the camshaft. Instantaneous and time-averaged values for pressure and temperature in each section of the engine were measured during engine tests. In order to ensure the validity of the tested data, all of the tests were conducted under fully-

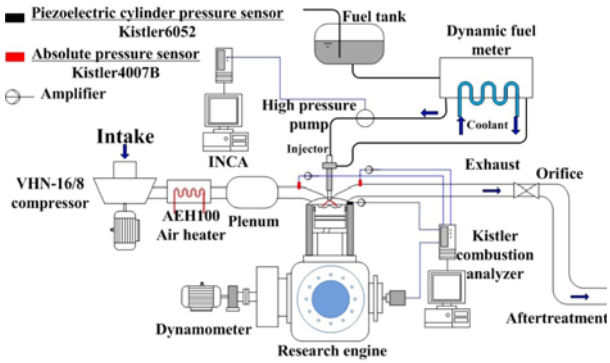

Figure 1. Schematic diagram of experimental setup.

warm engine running conditions and repeated three times in each operating condition.

2.2. Numerical Methods

2.2.1. Code and mesh domain

The shapes of the intake port and the combustion chamber were extruded by SPACECLAIM to create the 3D geometry. And then the CFD model was established with the commercial software CONVERGE (Convergent Science, 2014). The measured instantaneous intake/exhaust pressure and time-averaged values for temperature were taken as the boundary condition and initial condition of 3D simulation. In CONVERGE, the pressure-based transient solver was selected to allow a time dependent solution and the variable time-step algorithm was adopted. Viscous model k-epsilon (RNG) was also required to simulate turbulence. All the wall boundary has a grid scale of 2 and an embedded layer of 3. Thanks to the adaptive mesh refinement technology (AMR), we can set the wall boundary grid scale as 4 if the y-plus > 300. Then, the cell number in the domain was changed by adjusting the base grid. The in-cylinder pressure simulation results of the meshes smaller than 4 mm varied little, as shown in Figure 2 (b). So the base grid of 4 mm is adopted as a compromise of CPU time and accuracy, as shown in Figure 2 (a). The number of cells in the domain is 1400000 at the BDC.

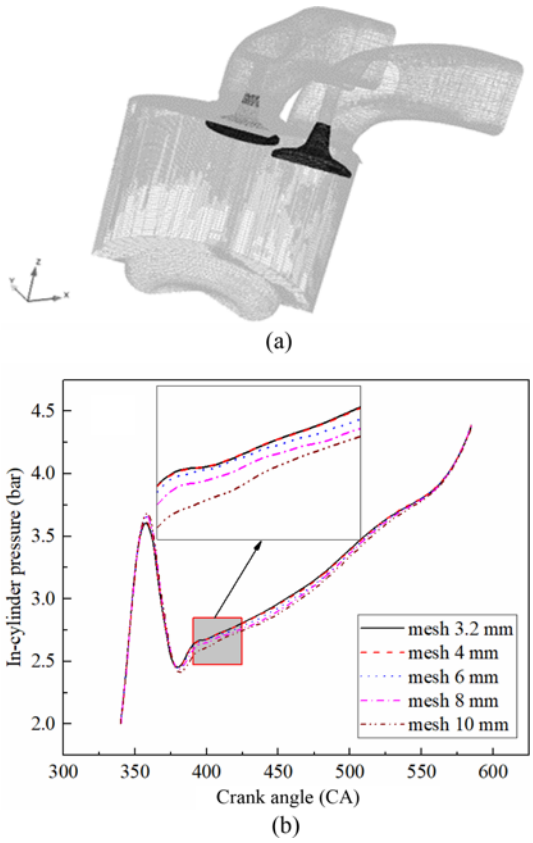

Figure 2. Computational meshes and sensitivity analysis results of the base grid: (a) Computational domain and mesh model; (b) In-cylinder pressure results with different base grid (2500 r/min).

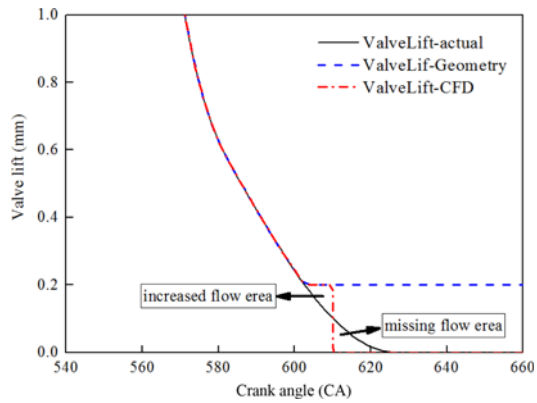

Figure 3. Valve profile of CFD simulation.

In CFD model, the valve and the valve seat do not contact fully when the valve is closed but maintains a minimum clearance to prevent an intersecting surface error. In this paper, the minimum clearance lift is 0.2 mm which is recommended by CONVERGE. And the valve closing event was controlled to occur at half of the minimum lift, as shown in Figure 3. The reason for doing so is to compensate the missing flow area after CFD valve closing by creating a large flow area before the CFD valve closing (Senecal *et al*., 2007; Yang *et al*., 2016).

2.2.2. Validation of the model

As shown in Figure 4, the validation of the simulation model was judged based on whether the CFD pressure trace matches the average in-cylinder pressure measured in the test bench during the pumping loop with an engine speed of 2500 r/min and intake mean absolute pressure of 3.5 bar. The mean error for this model is 3.61 % over the whole simulated range, which is lower than 4.5 % used by

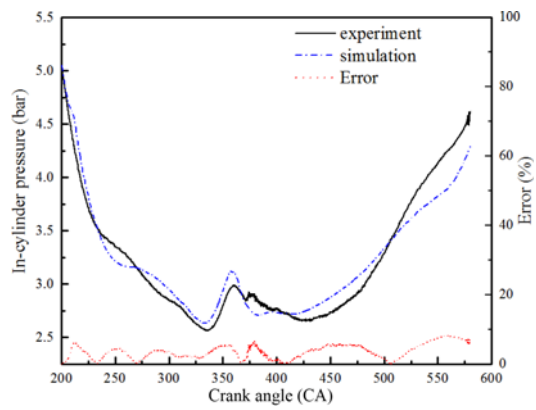

Figure 4. Comparison between experiment and simulation for the pumping pressure loop (2500 r/min).

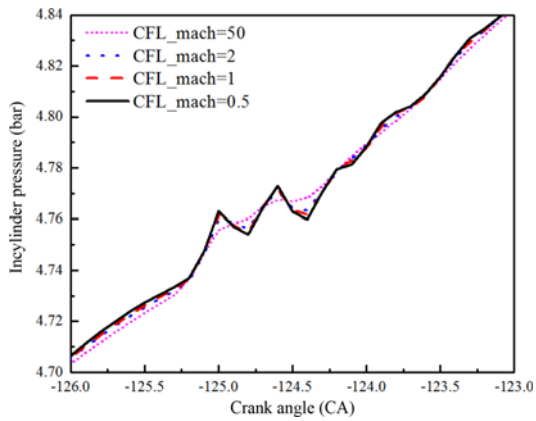

Figure 5. Calculated in-cylinder pressure oscillation with different CFL_mach numbers.

Mahrous *et al*. (2009) and Clenci *et al*. (2014). Therefore, the calculated data have shown a satisfying agreement to the measured data, and the maximum relative error during the pumping loop is controlled below 8 %.

The maximum Mach Courant Friedrichs-Lewy (CFLmach), which is based on the sound velocity, was adjusted. As shown in Equation (1), small numbers of CFLmach results in a small time step, making it more possibly to accurately catch the short-term pressure fluctuations whose velocity is the same as the sound.

$$CFLmach = c\,\frac{\Delta t}{\Delta x} \tag{1}$$

The calculated in-cylinder pressure fluctuation with different CFLmach numbers are shown in Figure 5. For the given mesh, although the pressure oscillation can be captured by every setup of the CFLmach, the amplitude of the pressure oscillation varied little in cases whose CFLmach is lower than 1. So, CFLmach = 1 was used for evaluation in all the cases.

3. EXPERIMENTAL RESULTS

3.1. Pressure Oscillation Signal

To prevent ignoring high frequency but small amplitude pressure oscillations, we did not average the in-cylinder pressure data. The 80th of 100 cycles was selected in order to exclude the incomplete records due to the long time for the pneumatic controlled exhaust pressure sensors to switch on or off. Figure 6 (a) shows the 80th in-cylinder pressure evolution of the 100 cycles at 2500 r/min, full load condition. As shown in Figure 6 (a), there exists a high frequency pressure fluctuation along the in-cylinder pressure traces during the compression stroke. The fluctuation first occurs suddenly with a relatively bigger amplitude, then, the amplitude becomes smaller and smaller, until invisible. For the reason of clarity, Figure 6 (b) only presents the 1st, 20th, 40th, 60th, 80th, and 100th pressure traces of 100 cycles. Although only the 80th of the

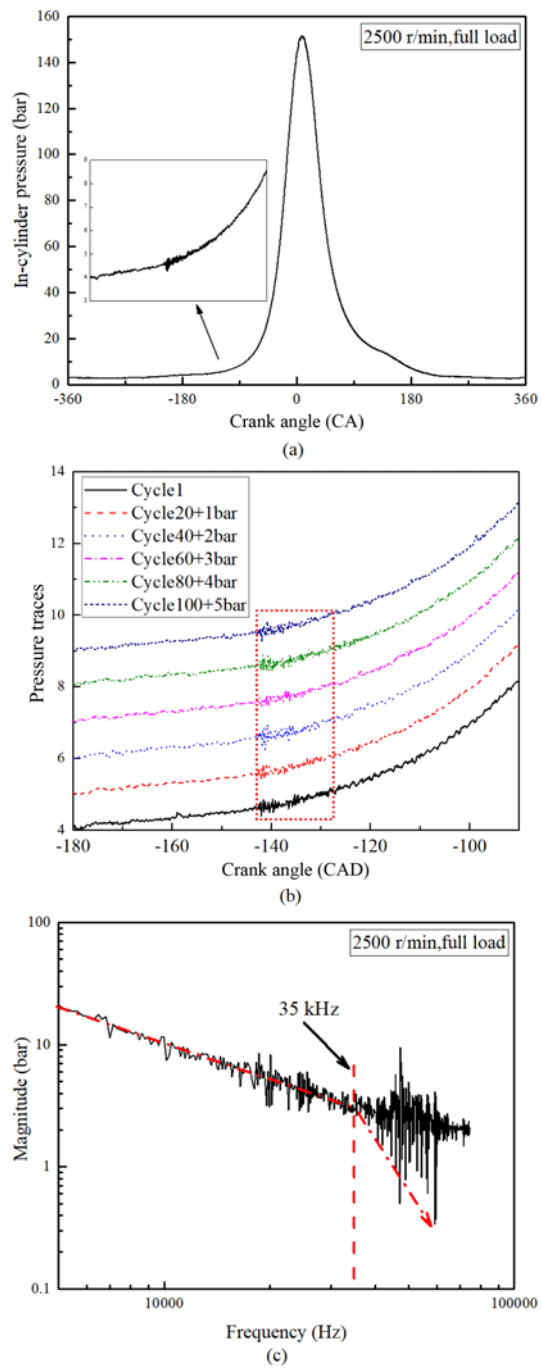

Figure 6. In-cylinder pressures at 2500 r/min, full load condition: (a) In-cylinder pressure and pressure oscillation phenomenon during the compression stroke; (b) Six pressure traces of the 100 cycles; (c) In-cylinder pressure spectrum.

100 record pressure traces is selected as a representative to study the oscillation, as Figure 6 (b) shows, all the 100 cycles of in-cylinder pressures record the pressure oscillation clearly.

As the main theme of the present study is the pressure

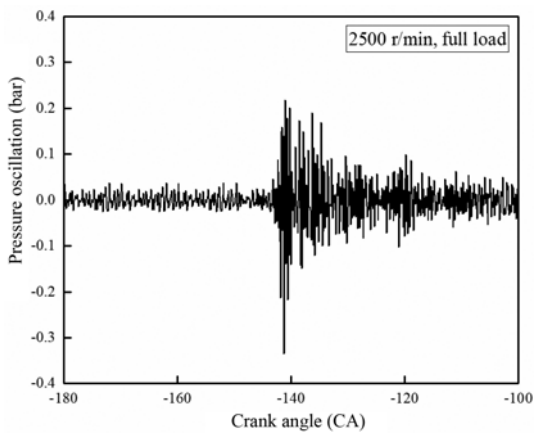

Figure 7. Obtained pressure oscillation signal.

oscillation during the compression stroke, the other pressure oscillations caused by pilot combustion, main combustion, and so on, are excluded by choosing the early half of compression stroke (− 180 CAD ~ − 90 CAD) as the time window. The in-cylinder pressure spectrums are obtained through the fast Fourier transformation (FFT) of the signals during the time window. As shown in Figure 6 (c), the pressure spectrum shows that the amplitude of the in-cylinder pressure decreases linearly as the frequency rises on logarithmic coordinate below 35 kHz, while oscillates violently after 35 kHz. Furthermore, as the red arrow in Figure 6 (c) illustrates, the minimum magnitude decreases with a larger slope rate after 35 kHz, comparing with the data before 35 kHz. Therefore, the 35 kHz is the critical frequency of the pressure oscillation. The similar criteria is also used by Zhang *et al*. (2017). So, the initial pressure data in the time window is passed through a digital high pass filter (cut-off frequency: 35 kHz) to firstly get the filtered pressure signals. Then, the pressure oscillation signals is obtained by subtracting the filtered pressure signals from the initial pressure data. The obtained pressure oscillation signal is shown in Figure 7.

3.2. Pressure Oscillations at Different Engine Speeds

When diesel engine operates under different engine speeds, the different air intake mass and the air flow velocity result in different gas characteristics, such as the pressure, density and temperature during the occurrence of the pressure oscillation. These will have some effects on the intensity and frequency characteristics of the pressure oscillation.

Figure 8 (a) shows the in-cylinder pressure at different engine speeds under full load condition. When the engine speed rises, the in-cylinder pressure decreases due to the lower intake pressure at high engine speed. The pressure fluctuation at 2100 r/min and 1900 r/min is more violent than that at 1600 r/min. As Figure 8 (b) shows, as same with Figure 6 (c), the amplitude of the in-cylinder pressure at 2100 r/min decreases linearly as the frequency rises on logarithmic coordinate below 35 kHz, while oscillates violently after 35 kHz. Furthermore, the minimum magnitude decreases with a larger slope rate after 35 kHz,

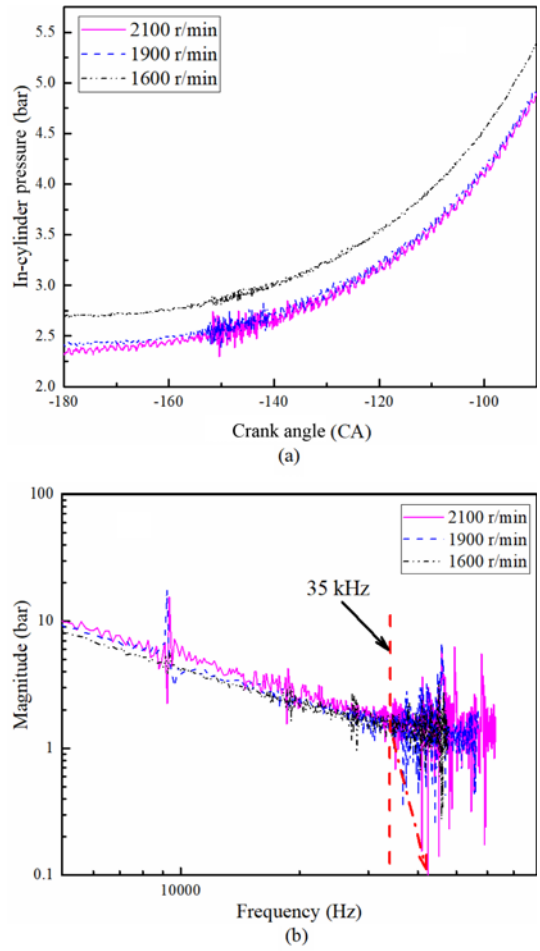

Figure 8. In-cylinder pressure at different engine speeds under full load condition: (a) In-cylinder pressure evolution; (b) In-cylinder pressure spectrum.

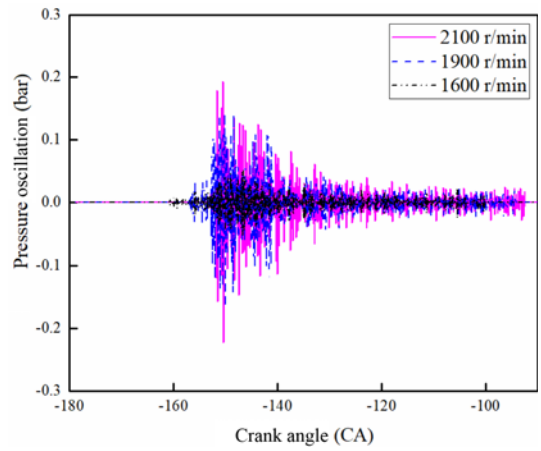

Figure 9. Pressure oscillation signals at different engine speeds.

comparing with the data before 35 kHz. Therefore, the 35 kHz is also the critical frequency of the pressure oscillations at 2100 r/min. The amplitude of all pressure fluctuations at different engine speeds rises since 35 kHz. It also can be found that, for 1600 r/min and 1900 r/min, the amplitude of the in-cylinder pressure decreases linearly below 35 kHz except the 10 kHz. This frequency is an abnormal signal that should be ignored.

The pressure oscillation signals at different engine speeds are presented in Figure 9. The shapes of the pressure oscillations are similar: the amplitude of all engine speeds reaches its maximum at the same crank angle very quickly and then attenuate to zero. However, the amplitude and the duration of the pressure oscillation rises as the engine speed rises. The amplitude of 2100 r/min is maximum, followed by the 1900 r/min, and finally is the 1600 r/min. And so as the duration. As the engine speed increases from 1600 r/min to 2100 r/min, the amplitude of the pressure oscillation increases from 0.05 bar to 0.2 bar.

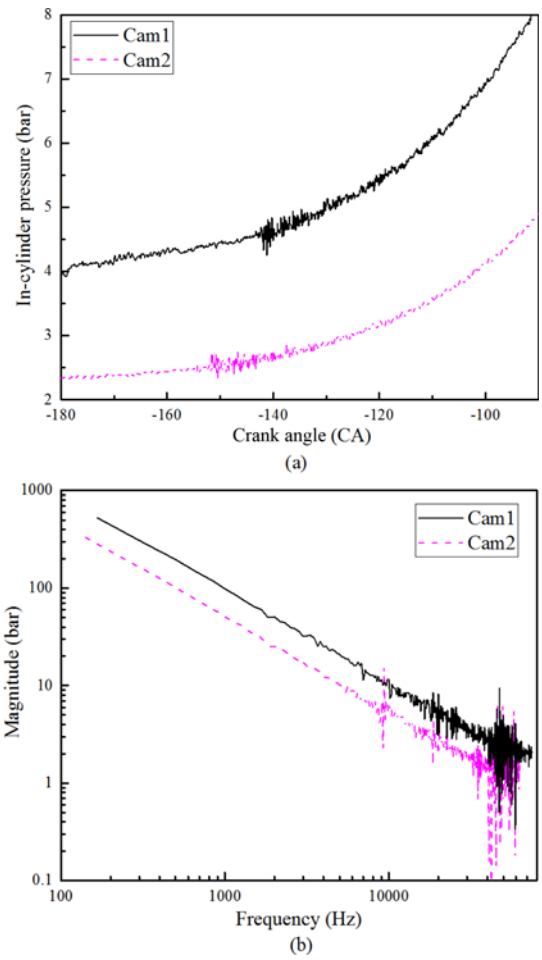

Figure 10. In-cylinder pressure at different IVC timings: (a) In-cylinder pressure evolution; (b) In-cylinder pressure spectrum.

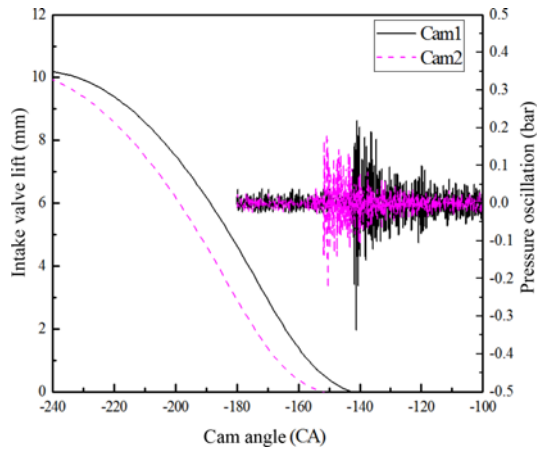

Figure 11. Intake valve lift and pressure oscillation signal at different IVC timings.

3.3. Pressure Oscillations at Different IVCs

Judging from above section, the engine speed has little effects on the timing of the pressure fluctuation occurrence. So, the source of the pressure fluctuation is very likely originated from a "cycle related" events. Figure 10 presents the in-cylinder pressure and the spectrum under 2100 r/min at different cams. According to the intake valve lifts in Figure 11, the main difference between cam1 and cam2 is the IVC timing: the IVC of the cam2 is 10 CAD earlier than that of the cam2. As Figure 10 (b) shows, the critical frequency of in-cylinder fluctuations for both IVCs is 35 kHz. However, the frequency related to the maximum amplitude for Cam1 is bigger than that for Cam2. That is to say, the frequency of the pressure fluctuation decreases as the IVC advances.

The pressure oscillation results are shown in Figure 11. It can be found that the pressure oscillation amplitude of Cam1 is bigger than that of Cam2, which means that the pressure oscillation source energy of Cam1 is bigger than Cam2. In addition, the designed IVC timing for the cam1 and cam2 can be distinguished according to the intake valve lift curve. The IVC timing of cam1 is – 143.5 CADand that of cam2 is – 153.5 CAD. When the IVC timing advances, the start time of the pressure oscillation advances too. The start time of the pressure oscillation corresponding to cam1 and cam2 is – 140 CAD and – 150 CAD, respectively. Consequently, it is can be concluded that the appearance of the pressure oscillation is caused by the IVC events.

4. DISCUSSIONS

Although we have learned that the in-cylinder pressure oscillation is excited by the closing event of the intake valve, we must study the pressure oscillation further for two reasons. First, the intake valve lift in Figure 11 is the designed one with an ideal valve lash of 0.25 mm. When the engine is running, the real IVC timing is unknown due

to the metal heat bilges, the reserved valve clearance and the inertia of the components. So, the time delay between the IVC and the start of the pressure oscillation cannot be determined by experiments. Secondly, with limited experimental data and many interfering signals, we can only get some superficial tendencies (such as the advance of IVC will result in a decrease of amplitude and a decrease of frequency), but the fundamental mechanisms for those tendencies are unknown. Therefore, in the present paper, the CFD model is used to further study the pressure oscillation.

4.1. In-cylinder Pressure Oscillation in CFD Model

The pressure oscillation is reproduced in CFD model for the case of IVC = – 126. In order to visualize the flow velocity field and the pressure field at the intake gap, the 3D model is cut with a plane (see Figure 12), which is parallel to the cylinder axis and passes the center of the intake valve and the center of the monitor point. To obtain the local absolute pressure, the monitor point is set at the same position with the in-cylinder pressure sensor, as the black point shows in Figure 12. Since the position of the in-cylinder pressure sensor hasn't been changed during experiment, the closest distance from the inner ring of the intake valve seat to the position of the in-cylinder pressure sensor (d, in Figure 12) maintains constant as 12.5 mm.

The two-dimensional graph (2D) curves in the bottom right corner of every subgraph in Figure 13 show the corresponding pressure traces of the monitor point. Before the IVC event happens, as shown in Figure 13 (a), the pressure field in the flow tunnel is determined by the flow structure: high speed results in low pressure. Hence, the air pressure at the intake valve gap is the lowest. It can also be found that the in-cylinder charge is pushed out of the cylinder due to the high in-cylinder pressure which is caused by the upward movement of the piston.

When the IVC event happens at – 126 CAD, as shown in Figure 13 (b), the backflow is stopped. It can be found that a high pressure/vacuum area appears at the in-cylinder/runner side of the intake valve, respectively. When the IVC event happens, since the intake flow that is still exiting the cylinder is stopped by the closure of the intake valve, the air downstream of the valve is still being pushed out of the cylinder volume due to inertia, as shown in Figure 13 (b). Due to the stagnation effect, the air flowing to the closed valve creates a high pressure at the area of valve sealing ring. Then, acting like a mass on a spring which is pulled down and then released, the pressure in the volume will overshoot and oscillate for a few cycles considering the air as an elastic fluid.

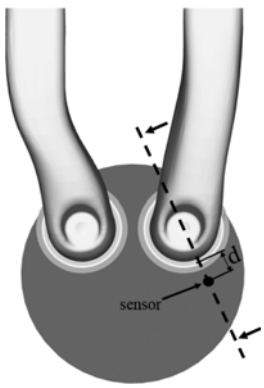

Figure 12. Positon of cutting plane and the in-cylinder pressure sensor.

According to Figure 13 (c), it can be found that 0.3 CAD later, the vacuum area in the runner becomes a little bigger, and so as the high pressure area in the cylinder. When the IVC event has happened after 0.5 CAD, as Figure 13 (d) shows, at the in-cylinder side of the intake valve, the high pressure originated from intake valve sealing gap spreads to the position of the monitor point. And it can be found that the point monitor captures the first pressure crest at this time, according to the 2D graph in Figure 13 (d). By contrast, the pressure vacuum at the runner side of the intake valve have left the valve sealing surface and traveled for a small distance.

Judging from Figure 13 (e), the monitor point captures the second pressure crest at 0.9 CAD after the close event happens. Apparently, two pressure crests and two pressure troughs can be seen at the in-cylinder side and the runner side of the intake valve, respectively. And it can be seen that the pressure wave spreads in a spherical way. Also, the third, fourth, and fifth pressure crest can be clearly recorded in Figures 13 (f) and (g). Due to the viscous and turbulent dissipation, the amplitude of the oscillation is the biggest at the first moment of its appearance and gradually decreases, except the fourth pressure crest. The reason why the amplitude of the fourth pressure crest is higher than the second, and the third pressure crest is that the first pressure crest generated by the right side of the valve gap (as A shown in Figure 13 (c)) and the fourth pressure crest generated by the left side of the valve gap (as B shown in Figure 13 (c)) are superimposed at the monitoring point.

4.2. Effect of IVC on Pressure Oscillation

To study the impacts of IVC on the pressure oscillation, the pressure of the CFD monitoring point is recorded at 2500 r/min, with different IVCs and fixed IVO, as shown in Figure 14 (a).

After the same filtering method as the experiment adopted, the pressure oscillations for different IVCs is shown in Figure 14 (b). The black spots on each pressure oscillation curve represent the amplitude of the first pressure peak. The spots above the horizontal axis indicate when the pressure crest first happens. By contrast, the spots bellow the horizontal axis indicate when the pressure trough first happens. After understanding the methodology of the in-cylinder pressure oscillation, it could be concluded that the first pressure crest at the in-cylinder side is due to the backflow from the cylinder to the intake

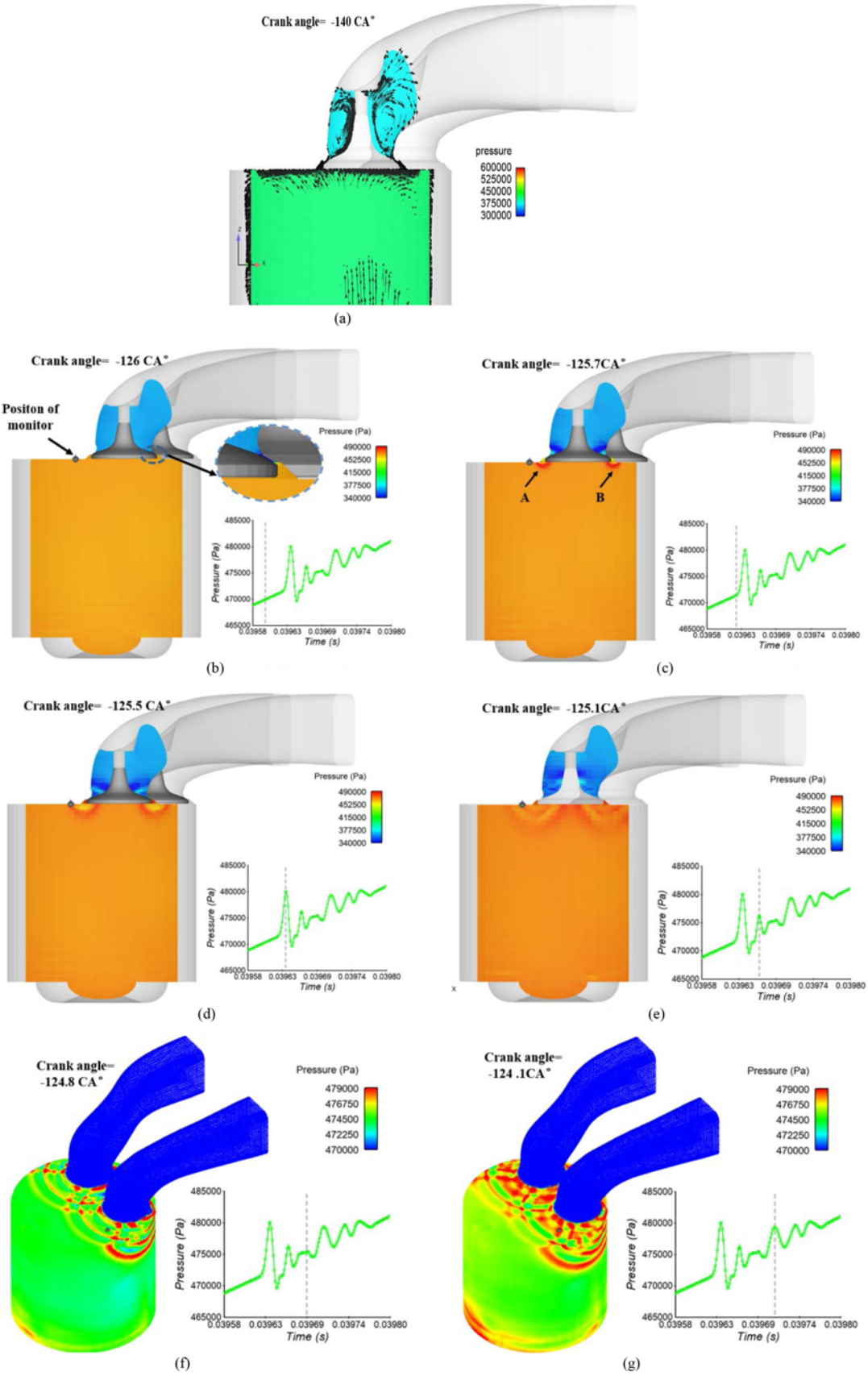

Figure 13. Pressure fields for case IVC = – 126.

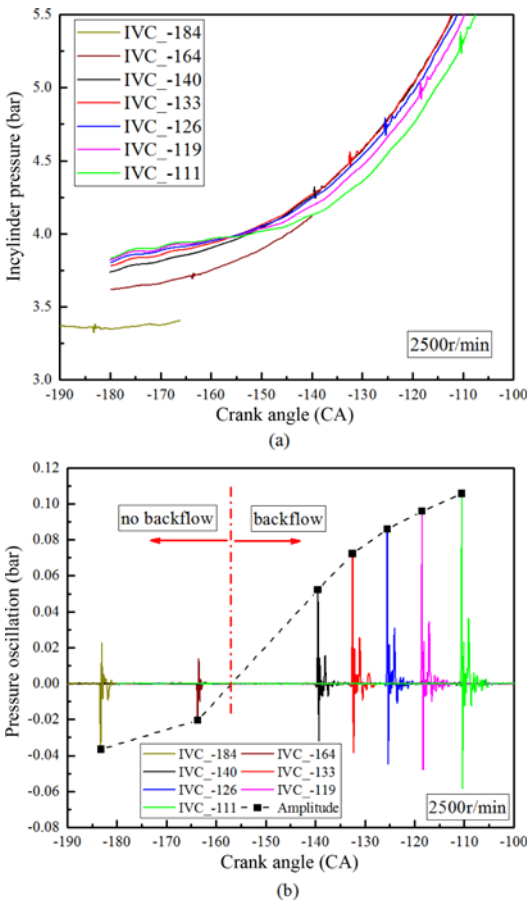

Figure 14. In-cylinder pressure at different IVCs: (a) In-cylinder pressure evolution; (b) Pressure oscillation.

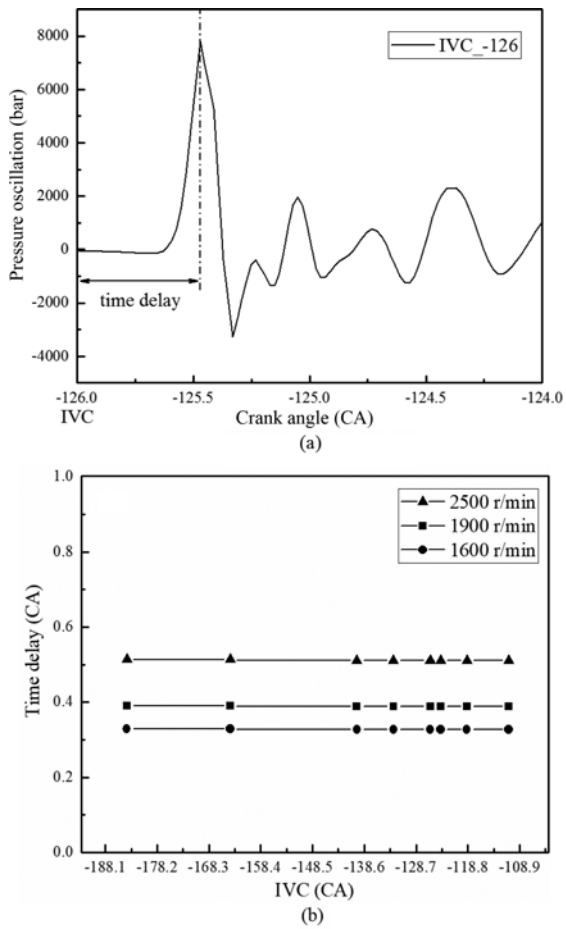

Figure 15. (a) Definition of the time delay; (b) Time delays for different engine speeds.

runner. Hence, it is reasonable to conclude that the forward flow will result in a first pressure trough at the in-cylinder side. As Figure 14 (b) illustrates, there exists backflow for cases IVC = – 140, – 133, – 126, – 119, and – 111, whereas no backflow happens for the cases IVC = – 184 and IVC = – 164.2.

It can also be found in Figure 14 (b) that the amplitude of the pressure oscillation decreases as the IVC retards when no backflow happens. However, when there exists backflow, the amplitude of the pressure oscillation increases as the IVC retards, showing an opposite trend with the none-backflow situation. A reasonable explanation for this trend is that the energy of the pressure oscillation is originated from the inertia of the moving air. When there is no backflow, the forward air velocity decreases as the IVC retards due to the decreasing pressure difference between the cylinder and intake runner. By contrast, when there exists backflow, the later the intake valves close, the bigger the pressure difference created by the additional volume being displaced by the piston is. And big pressure difference results in a high backflow velocity. Therefore, a retarded IVC will cause a pressure oscillation with bigger amplitude.

To determine the relationship between the IVC events and the pressure oscillation, the time delay between the IVC events and the time when the pressure oscillation amplitude first reaches its maximum is defined, as shown in Figure 15 (a). Taking the maximum point of pressure amplitude as a reference point is because the pressure sensor is most likely to capture this signal.

The crank angle delay as a function of IVC timing is shown in Figure 15 (b). It can be found that the time delay keeps constant in a quite long range of IVC. The time delay in crank angle are 0.327 CAD, 0.388 CAD, and 0.511 CAD for 2500 r/min, 1900 r/min, and 1600 r/min, respectively. When the unit of time delay is converted to seconds, the time delay is uniformly 34 microseconds for all the cases. So, it can be concluded that the IVC event and the engine speed have little influence on the delay. In other word, the delay and the IVC events are independent of each other.

Although the engine speed has no influence on the absolute time delay, it will affect the crank angle time delay. However, we cannot see this difference in the experimental data in Figure 9. This is mainly due to that the time delay is too short. For a time delay of 34

microseconds, the crank angle difference between the 2500 r/min and the 1600 r/min is only 0.18 CAD, which is very difficult to distinguish in the experiment.

4.3. Potential Applications

Since the characteristics of the in-cylinder pressure oscillation have been analyzed above, the potential application of the findings will be discussed below.

The first potential application of the in-cylinder pressure oscillation is to monitor the IVC timing in a running engine. Once the time delay can be determined by simple formula, the online measuring of the valve event will be much easier. Time delay is actually the time that the first pressure crest (trough) travels from generation to propagation to the pressure monitoring point. It has been found that the velocity of the pressure wave is equal to the sound speed, which is related to the gas temperature. For ideal gas, the sound speed is approximately computed by $c = \sqrt{\gamma RT}$, where the g is the adiabatic coefficient and R is the gas constant. So, the time delay can be calculated by:

$$\Delta T = \frac{d}{\sqrt{\gamma RT}} \tag{2}$$

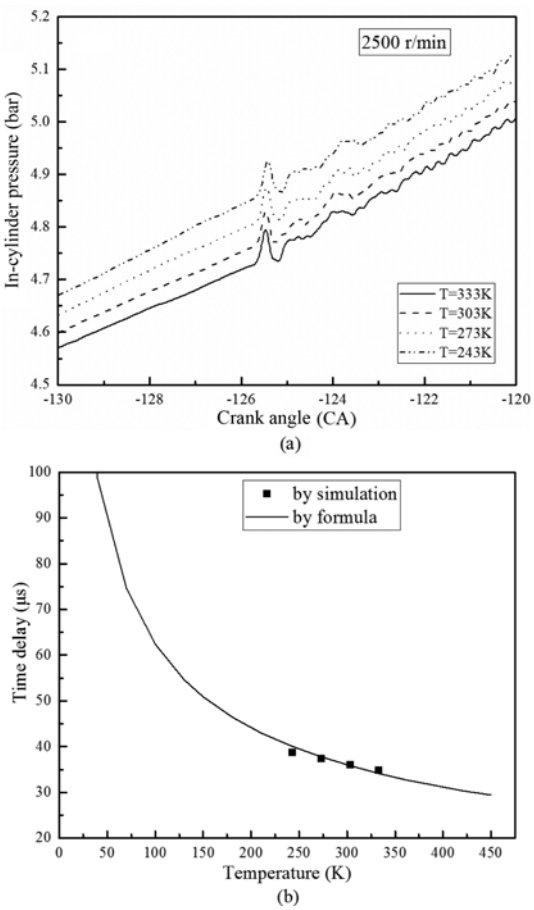

Figure 16. In-cylinder pressure at different intake air temperatures: (a) In-cylinder pressure evolution; (b) Time delay.

In the present study, the distance d is fixed as constant of 12.5 mm (see Figure 12). g and R are constants for the air. Therefore, the time delay is highly dependent on the intake air temperature. The simulated in-cylinder pressure fluctuations for different intake air temperatures are shown in Figure 16 (a). The time delay and the calculated time delay by Equation (2) at different intake air temperatures are presented in Figure 16 (b). As the intake temperature increases from 243 K to 333 K, the time delay decreases from 39 microseconds to 34 microseconds. From Figure 16 (b), it can be found that the formula matches the simulated results well. As this formula is free of complex computation, it is easy to realize in a real engine. By this means, the real IVC timing can be monitored when the engine is running. Moreover, in the PCCI or HCCI engines, the EIVC or LIVC strategy is adopted to control the SOC of these engines. With the EIVC or LIVC strategy, the pressure oscillation phenomenon will be much easier to detect due to that the air velocity at the valve gap is higher. So, this method will provide a new and prospective method to monitor the online IVC timing, and then, predictive SOC controlling in PCCI&HCCI engines is possible.

The second potential application of the in-cylinder pressure oscillation is to determine the optimal IVC timing, which makes the air that ends up in the cylinder the most. According to the reference (Pulkrabek, 1997), the ideal time for the intake valve to close is when the air start to change its direction but not change. As shown in Figure 14 (b), the shape of the pressure oscillation is dependent on the air flow direction. As the IVC retards, the amplitude of the pressure oscillation decreases when no backflow happens and increases when there exists backflow. In Figure 11, the amplitude of the pressure oscillation in the real single cylinder engine increases as the IVC retards. So, it can be concluded that the backflow happens for both two cams and that the IVC timing should advance for this engine to trap the maximum air.

Consequently, deeply understanding on the pressure oscillation can be truly helpful for the improvement of the solution of predictive SOC controlling in PCCI/HCCI engines, and the improvement of engine performance.

5. CONCLUSION

In this paper, the in-cylinder pressure fluctuation phenomenon during the compression stroke for a single-cylinder diesel engine has been investigated by combined experiment and CFD simulation. Based on the experimental and simulation investigations, the following conclusions can be drawn:

(1) The experimental results show that the occurrence of pressure fluctuation is highly related to the IVC timing. The simulation results reveal that the appearance of the in-cylinder pressure oscillation is due to the cut-off of the intake flow by the IVC event. High engine speed results in a bigger fluctuation amplitude and a longer

fluctuation duration. As the engine speed increases from 1600 r/min to 2100 r/min, the amplitude of the pressure oscillation increases from 0.05 bar to 0.2 bar.

(2) At the same engine speed, as IVC retards, the air that is induced into cylinder changes its direction. And the amplitude of the pressure oscillation decreases first and then increases as the IVC retards. The 35 kHz is the critical frequency of the pressure oscillation. As the intake temperature increases from 243 K to 333 K, the time delay decreases from 39 microseconds to 34 microseconds. With the same intake temperature, the absolute time delay keeps constant at different engine speed and different IVC timings.

(3) Two potential applications of this phenomenon are discussed in detail. Firstly, it can be used to monitor the online IVC timing on a running engine, which is essential for the PCCI/HCCI engines to control the SOC of these engines precisely in the whole working range. Secondly, the ideal IVC timing can be determined according to the amplitude of the pressure oscillation.

ACKNOWLEDGEMENT–The authors would like to acknowledge the financial support provided by the Beijing Natural Science Foundation (Grant No.: 3174055) and the National Natural Science Foundation of China (Grant No.: 51606010).

REFERENCES

Beccari, S., Pipitone, E. and Genchi, G. (2016). Knock onset prediction of propane, gasoline and their mixtures in spark ignition engines. *J. Energy Institute* **89**, **1**, 101–114.

Bodisco, T., Reeves, R., Situ, R. and Brown, R. (2012). Bayesian models for the determination of resonant frequencies in a DI diesel engine. *Mechanical Systems and Signal Processing*, **26**, 305–314.

Bozza, F., De Bellis, V. and Teodosio, L. (2016). Potentials of cooled EGR and water injection for knock resistance and fuel consumption improvements of gasoline engines. *Applied Energy*, **169**, 112–125.

Brijesh, P. and Sreedhara, S. (2013). Exhaust emissions and its control methods in compression ignition engines: A review. *Int. J. Automotive Technology* **14**, **2**, 195–206.

Clenci, A. C., Iorga-Simăn, V., Deligant, M., Podevin, P., Descombes, G. and Niculescu, R. (2014). A CFD (Computational Fluid Dynamics) study on the effects of operating an engine with low intake valve lift at idle corresponding speed. *Energy*, **71**, 202–217.

Convergent Science, I. (2014). CONVERGE Version 2.2 Theory Manual. USA.

Flett, J. and Bone, G. M. (2016). Fault detection and diagnosis of diesel engine valve trains. *Mechanical Systems and Signal Processing*, **72-73**, 316–327.

Fog, T. L., Hansen, L. K., Larsen, J., Hansen, H. S., Madsen, L. B., Sorensen, P., Hansen, E. R. and Pedersen, P. S. (1999). On condition monitoring of exhaust valves in marine diesel engines. *Neural Networks for Signal Processing IX: Proc. IEEE Signal Processing Society Workshop (Cat. No. 98TH8468)*. Madison, Wisconsin, USA.

Ftoutou, E., Chouchane, M. and Besbès, N. (2011). Internal combustion engine valve clearance fault classification using multivariate analysis of variance and discriminant analysis. *Trans. Institute of Measurement and Control* **34**, **5**, 566–577.

Hickling, R., Feldmaier, D. A., Chen, F. H. K. and Morel, J. S. (1983). Cavity resonances in engine combustion chambers and some applications. *J. Acoustical Society of America* **73**, **4**, 1170–1178.

Hickling, R., Hamburg, J. A., Feldmaier, D. A. and Chung, J. Y. (1979). Method of Measurement of Bulk Temperatures of Gas in Engine Cylinders. Patent No. US4164867A.

Jia, M., Li, Y., Xie, M. and Wang, T. (2013). Numerical evaluation of the potential of late intake valve closing strategy for diesel PCCI (Premixed Charge Compression Ignition) engine in a wide speed and load range. *Energy*, **51**, 203–215.

Jia, M., Xie, M., Wang, T. and Peng, Z. (2011). The effect of injection timing and intake valve close timing on performance and emissions of diesel PCCI engine with a full engine cycle CFD simulation. *Applied Energy* **88**, **9**, 2967–2975.

Kyrtatos, P., Brückner, C. and Boulouchos, K. (2016). Cycle-to-cycle variations in diesel engines. *Applied Energy*, **171**, 120–132.

Li, N., Xie, H., Chen, T., Li, L. and Zhao, H. (2013). The effects of intake backflow on in-cylinder situation and auto ignition in a gasoline controlled auto ignition engine. *Applied Energy*, **101**, 756–764.

Li, X., Gao, H., Zhao, L., Zhang, Z., He, X. and Liu, F. (2016). Combustion and emission performance of a split injection diesel engine in a double swirl combustion system. *Energy*, **114**, 1135–1146.

Li, Y., Tse, P. W., Yang, X. and Yang, J. (2010). EMD-based fault diagnosis for abnormal clearance between contacting components in a diesel engine. *Mechanical Systems and Signal Processing* **24**, **1**, 193–210.

Liu, F. S., Sun, B. G., Zhu, H. R., Hu, T. G., Du, W., Li, X. R. and Zhang, Z. (2014). Development of performance and combustion system of Atkinson cycle internal combustion engine. *Science China-Technological Sciences* **57**, **3**, 471–479.

Liu, F., Shi, Z., Hua, Y., Kang, N., Li, Y. and Zhang, Z. (2018). Study on the intake valve close timing misalignment between the maximum volume efficiency and the none backflow on a single cylinder diesel engine. *J. Engineering for Gas Turbines and Power* **141**, **2**, 021026-1–021026-10.

Lu, X., Han, D. and Huang, Z. (2011). Fuel design and management for the control of advanced compression-

ignition combustion modes. *Progress in Energy and Combustion Science* **37**, **6**, 741–783.

Luján, J. M., Guardiola, C., Pla, B. and Bares, P. (2016). Estimation of trapped mass by in-cylinder pressure resonance in HCCI engines. *Mechanical Systems and Signal Processing*, **66-67**, 862–874.

Mahrous, A. F. M., Potrzebowski, A., Wyszynski, M. L., Xu, H. M., Tsolakis, A. and Luszcz, P. (2009). A modelling study into the effects of variable valve timing on the gas exchange process and performance of a 4-valve DI Homogeneous Charge Compression Ignition (HCCI) engine. *Energy Conversion and Management* **50**, **2**, 393–398.

Milovanovic, N., Chen, R. and Turner, J. (2004). Influence of variable valve timings on the gas exchange process in a controlled auto-ignition engine. *Proc. Institution of Mechanical Engineers, Part D: J. Automobile Engineering* **218**, **5**, 567–583.

Nivesrangsan, P., Steel, J. A. and Reuben, R. L. (2005). AE mapping of engines for spatially located time series. *Mechanical Systems and Signal Processing* **19**, **5**, 1034–1054.

Nivesrangsan, P., Steel, J. A. and Reuben, R. L. (2007a). Acoustic emission mapping of diesel engines for spatially located time series – Part II: Spatial reconstitution. *Mechanical Systems and Signal Processing* **21**, **2**, 1084–1102.

Nivesrangsan, P., Steel, J. A. and Reuben, R. L. (2007b). Source location of acoustic emission in diesel engines. *Mechanical Systems and Signal Processing* **21**, **2**, 1103–1114.

Peng, Z. J. and Jia, M. (2009). Full engine cycle CFD investigation of effects of variable intake valve closing on diesel PCCI combustion and emissions. *Energy Fuels* **23**, **12**, 5855–5864.

Pulkrabek, W. W. (1997). *Engineering Fundamentals of the Internal Combustion Engine*. 2nd edn. Prentice Hall. Upper Saddle River, New Jersey, USA.

Reuben, R. L. (1998). The role of acoustic emission in industrial condition monitoring. *Int. J. Comadem* **1**, **4**, 35–46.

Senecal, P. K., Richards, K. J., Pomraning, E., Yang, T., Dai, M. Z., McDavid, R. M., Patterson, M. A., Hou, S. and Shethaji, T. (2007). A new parallel cut-cell cartesian CFD code for rapid grid generation applied to in-cylinder diesel engine simulations. *SAE Paper No*. 2007-01-0159.

Tougri, I., Colaço, M. J., Leiroz, A. J. K. and Melo, T. C. C. (2017). Knocking prediction in internal combustion engines via thermodynamic modeling: Preliminary results and comparison with experimental data. *J. Brazilian Society of Mechanical Sciences and Engineering* **39**, **1**, 321–327.

Vafamehr, H., Cairns, A., Sampson, O. and Koupaie, M. M. (2016). The competing chemical and physical effects of transient fuel enrichment on heavy knock in an optical spark ignition engine. *Applied Energy*, **179**, 687–697.

Walter, B., Pacaud, P. and Gatellier, B. (2008). Variable valve actuation systems for homogeneous diesel combustion: How interesting are they?. *Oil & Gas Science and Technology - Rev. IFP* **63**, **4**, 517–534.

Wang, C., Zhang, Y. and Zhong, Z. (2008). Fault diagnosis for diesel valve trains based on time-frequency images. *Mechanical Systems and Signal Processing* **22**, **8**, 1981–1993.

Wu, W., Lin, T. R. and Tan, A. C. C. (2015). Normalization and source separation of acoustic emission signals for condition monitoring and fault detection of multi-cylinder diesel engines. *Mechanical Systems and Signal Processing*, **64-65**, 479–497.

Xu, G. F., Jia, M., Li, Y. P., Xie, M. Z. and Su, W. H. (2017). Multi-objective optimization of the combustion of a heavy-duty diesel engine with Low Temperature Combustion (LTC) under a wide load range: (II) Detailed parametric, energy, and exergy analysis. *Energy*, **139**, 247–261.

Yang, X. F., Keum, S. and Kuo, T. W. (2016). Effect of valve opening/closing setup on computational fluid dynamics prediction of engine flows. *J. Engineering for Gas Turbines and Power* **138**, **8**, 081503-1–081503-16.

Yao, M., Zheng, Z. and Liu, H. (2009). Progress and recent trends in homogeneous charge compression ignition (HCCI) engines. *Progress in Energy and Combustion Science* **35**, **5**, 398–437.

Zhang, Q., Hao, Z., Zheng, X. and Yang, W. (2017). Characteristics and effect factors of pressure oscillation in multi-injection DI diesel engine at high-load conditions. *Applied Energy*, **195**, 52–66.

Publisher's Note Springer Nature remains neutral with regard to jurisdictional claims in published maps and institutional affiliations.